Applied Surface Science 434 (2018) 1336–1343

Contents lists available at ScienceDirect

Applied Surface Science

journal homepage: www.elsevier.com/locate/apsusc

Full Length Article

Room-temperature processed tin oxide thin film as effective hole blocking layer for planar perovskite solar cells

Hong Tao[a,*], Zhibin Ma[a], Guang Yang[b], Haoning Wang[c], Hao Long[c], Hongyang Zhao[a,d], Pingli Qin[b], Guojia Fang[b,*]

[a] Hubei Key Laboratory of Plasma Chemistry and Advanced Materials, School of Material Science and Engineering, Wuhan Institute of Technology, Wuhan, 430205, People's Republic of China
[b] Key Lab. of Artificial Micro- and Nano-Structures of Ministry of Education of China, School of Physics and Technology, Wuhan University, Wuhan, 430072, People's Republic of China
[c] College of Electronics and Information Engineering, South-Central University for Nationalities, Wuhan, 430074, People's Republic of China
[d] State Key Laboratory of Crystal Materials, Shandong University, Jinan, 250100, China

ARTICLE INFO

Article history:
Received 7 September 2017
Received in revised form
10 November 2017
Accepted 19 November 2017
Available online 22 November 2017

Keywords:
SnO_2
Magnetron sputtering
Room temperature
Hole blocking layer
Perovskite solar cell

ABSTRACT

Tin oxide (SnO_2) film with high mobility and good transmittance has been reported as a promising semiconductor material for high performance perovskite solar cells (PSCs). In this study, ultrathin SnO_2 film synthesized by radio frequency magnetron sputtering (RFMS) method at room temperature was employed as hole blocking layer for planar PSCs. The room-temperature sputtered SnO_2 film not only shows favourable energy band structure but also improves the surface topography of fluorine doped SnO_2 (FTO) substrate and perovskite ($CH_3NH_3PbI_3$) layer. Thus, this SnO_2 hole blocking layer can efficiently promote electron transport and suppress carrier recombination. Furthermore, the best efficiency of 13.68% was obtained for planar PSC with SnO_2 hole blocking layer prepared at room temperature. This research highlights the room-temperature preparation process of hole blocking layer in PSC and has a certain reference significance for the usage of flexible and low-cost substrates.

1. Introduction

Perovskite solar cell (PSC) has been developed greatly in recent years. The efficiency of perovskite solar cell has been increased to 22.1% from 9.7% in a very short period of time [1–6]. PSC was developed from the solid-state dye sensitized solar cell, and PSC with TiO_2 compact layer and mesoporous layer has achieved the highest efficiency of 22.1% [6]. Though PSC with mesoporous layer has advantages such as high efficiency and hysteresis-free, its complex and high-temperature preparation process still limits its development. Some researches have shown that perovskite materials can transport holes and electrons due to their great carrier diffusion lengths [2,7]. Therefore, meso-superstructured solar cell and planar PSC emerged and caused a lot of interest [2–4,8].

The most used hole blocking layer (HBL) in planar PSC is TiO_2 compact layer. However, TiO_2 film has some limitations such as high-temperature sintering process, low electron mobility and surface defect [9,10]. In order to lower the fabrication temperature, titanium oxide compact layer were prepared by some low-temperature technologies including solution method [11], physical deposition approach [12] and chemical bath deposition [13]. Doping [14] and modification [15] of TiO_2 film are also applied in planar PSC to improve its electron mobility and reduce its surface defect. In addition, some new oxide materials, such as Zn_2SnO_4, In_2O_3, WO_x, ZnO and SnO_2, are studied to replace TiO_2 compact layer in order to solve the above mentioned problems [16–20]. Among them, SnO_2 is a competitive substitution for TiO_2 because of its advantages such as low-temperature preparation, high electron mobility, wide band gap, suitable band structure and high transparency [9,20–26]. Therefore, there have been emerged many studies on the application of SnO_2 in PSC.

Ke et al. have demonstrated that low-temperature solution-processed SnO_2 film can make planar PSC achieve efficiency as high as 17.21%, in which SnO_2 thin film was annealed in air at 180 °C for 1 h [20]. SnO_2 film prepared by atomic layer deposition (ALD) under 118 °C was applied in planar PSC and showed a higher performance and better stability than TiO_2 film due to the deeper conduction band and barrier-free charge transport of SnO_2 film [24]. Microwave-assisted non-aqueous synthesized SnO_2

* Corresponding authors.
E-mail addresses: taohong@wit.edu.cn, 403824120@qq.com (H. Tao), gjfang@whu.edu.cn (G. Fang).

https://doi.org/10.1016/j.apsusc.2017.11.161
0169-4332/

nanocrystals were also applied in planar PSC and the reaction temperature was set as 130 °C [25]. In addition, Chen et al. utilized an electrochemical deposition technique to prepare SnO_2 films at a reduced temperature below 100 °C, and planar PSC based on this electrodeposited SnO_2 film showed efficiency up to 13.88% [26].

As mentioned above, low-temperature solution method is the most common method to prepare SnO_2 electron selective layer for PSC [20–23]. But the spin-coating method and thermal annealing still limit the application and industrialization of PSC. In addition, ALD technology requires a relatively long time and high-cost for the thin film preparation [12], which is also a limitation factor in terms of cost. Therefore, exploring the appropriate methods to prepare SnO_2 film for planar PSC is essential to the development of PSC. As we know, radio frequency magnetron sputtering (RFMS) is a low-cost method for preparing semiconductor thin films on various substrates and it is an alternative way to realize large area, low cost and commercialized devices [12]. RFMS method has been applied in the preparation process of PSC to enhance device performance, decrease preparation temperature and simplify fabrication technology [27–30]. And it can be utilized to deposite suitable electron transport layers and hole transport layers for both mesoporous and planar PSCs [27–30]. However, there are few reports about the research on the application of room-temperature sputtered SnO_2 film in planar PSC.

In this paper, SnO_2 thin film prepared by RFMS method at room-temperature is studied as hole-blocking layer (HBL) in planar PSC. Through this study, SnO_2 films with high mobility, good transmittance, wide band gap and suitable energy level position are prepared at room temperature. And these characteristics make planar PSC based on room-temperature sputtered SnO_2 HBL obtain excellent carrier transport and hole-blocking performance. In addition, this ultrathin SnO_2 film also contributes to the formation of smooth perovskite layer, which is crucial to the photoelectricity properties of PSCs. Finally, the efficiency of planar PSC with room-temperature sputtered SnO_2 HBL is optimized to 13.68%. This research demonstrates a room-temperature preparation method to prepare SnO_2 HBL in planar PSC, which is beneficial to the use of flexible and low-cost substrates.

2. Experimental section

2.1. Deposition of SnO_2 film

SnO_2 films were deposited on Fluorine-doped SnO_2 (FTO) conductive glasses via RFMS method. FTO glasses were washed in an ultrasonic bath using deionizer water, ethanol and acetone sequentially and then were dried under air atmosphere. The cleaned FTO substrates were fixed in vacuum chamber and SnO_2 target with a purity of 99.99% was also put into it. The distance between SnO_2 target and FTO substrate was approximately 60 mm. Before deposition, the chamber was evacuated to a pressure of 1×10^{-3} Pa. The sputtering atmosphere was consisted of argon (Ar) and oxygen (O_2). The gas flow rates of Ar and O_2 were controlled by gas-flow meters and the gas flow ratio of Ar and O_2 was set as 4:6. The sputtering process was under room temperature. The striking potential and sputtering potential were controlled as 3 Pa and 1 Pa, respectively. Then, 10 min pre-sputtering process was introduced before deposition in order to clean the surface of SnO_2 target. The SnO_2 target was sputtered with a sputtering power of 60 W. And the sputtering time was set as 20, 30 and 40 min (defined as sample RFMS-20, RFMS-30 and RFMS-40), respectively.

2.2. Fabrication of planar PSC

Bare FTO glass (defined as sample FTO) was used as the contrast sample. Perovskite ($CH_3NH_3PbI_3$) layer was deposited through two-step solution method. PbI_2 solution (462 mg/ml) was spin-coated on samples to form PbI_2 films in a glove box, and the solvent of PbI_2 solution contained 1 ml *N*,*N*-dimethylformamide (DMF) and 80 μl dimethyl sulfoxide (DMSO). The spin-coating speed was 2000 rpm for 45 s and the annealing condition of PbI_2 film was 70 °C for 30 min. After cooling down, PbI_2 films were dipped into CH_3NH_3I solution (10 mg/ml) for 5 min at 50 °C. Then, the samples were taken out and rinsed with cleaned isopropanol and annealed at 70 °C for 30 min. The hole transport material solution (HTM) containing 20 ml 4-tert-butylpyridine (TBP), 200 ml bis(trifluoromethane)sulfonimide lithium salt (LiTFSI), 2 ml chlorobenzene and 183.38 mg Spiro-OMeTAD was spin-coated on perovskite layer at 2000 rpm for 45 s. Finally, Au electrode was deposited on HTM layer via thermal evaporation method to form planar PSCs. And their active areas were 0.09 cm^2. The structure diagram of this planar PSC was shown in Fig. 1a.

2.3. Measurement of planar PSC

The morphology and roughness of samples were characterized by atomic force microscope (AFM, SPM-9500j3). The morphology of SnO_2 films and perovskite films were observed by scanning electron microscopy (SEM, JSM 6700F, Japan). The composition and kinetic energy spectrum of sputtered SnO_2 film were characterized by X-ray photoelectron spectroscopy (XPS) and ultraviolet photoelectron spectroscopy (UPS) methods using a XPS/UPS system (Thermo Scientific, Escalate 250Xi). The UV–vis transmission spectrum was measured with UV–vis-NIR spectrophotometer (Cary 5000, Varian). The electrical characteristics of sputtered SnO_2 films were measured by a LakeShore 7704 Hall Measurement System at room temperature. The photovoltaic characteristics of PSCs were measured by a CHI 660D electrochemical work station (Shanghai Chenhua Instruments, China) under illumination of simulated 100 mW cm^{-2} (AM 1.5) solar light from a solar simulator (ABET Sun 2000 Solar Simulator). Electrochemical impedance spectroscopy (EIS) was tested by the same CHI 660D electrochemical work station. The incident photon-to-electron conversion efficiency (IPCE) was measured as a function of wavelength from 300 to 800 nm by using a Model QE/IPCE system (PV Measurements Inc.).

3. Results and discussion

The mobility of SnO_2 film prepared by RFMS method is measured through hall measurement. Result indicates that the sputtered SnO_2 film has a high resistivity of 16,340 Ω cm and a superior mobility of 32.35 cm^2/Vs. The mobility of sputtered SnO_2 film is higher than that of traditional TiO_2 film, which can contribute to the relatively good performance of PSC [9]. The incremental carrier mobility can decrease the interfacial recombination rate of device, which has a positive effect on device performance [31,32]. In order to investigate the composition of room-temperature sputtered SnO_2 film, the sample sputtered on silicon substrate was observed by XPS and the result is shown in Fig. S1. The survey of full XPS spectra in Fig. S1a confirms the presence of Sn and O in sputtered SnO_2 film. The binding energies of 487.1 and 495.5 eV shown in Fig. S1b correspond to Sn $3d_{5/2}$ and Sn $3d_{3/2}$, which indicates that Sn is tetravalent in the sputtered film [20,33]. The scan of O 1s is shown in Fig. S1c and the main binding energy at 530.7 eV is attributed to O^{2-} state of sputtered SnO_2 film. And the peak at 531.9 eV belongs to chemisorbed oxygen atoms, hydroxide or oxy-hydroxide groups [20,24,33].

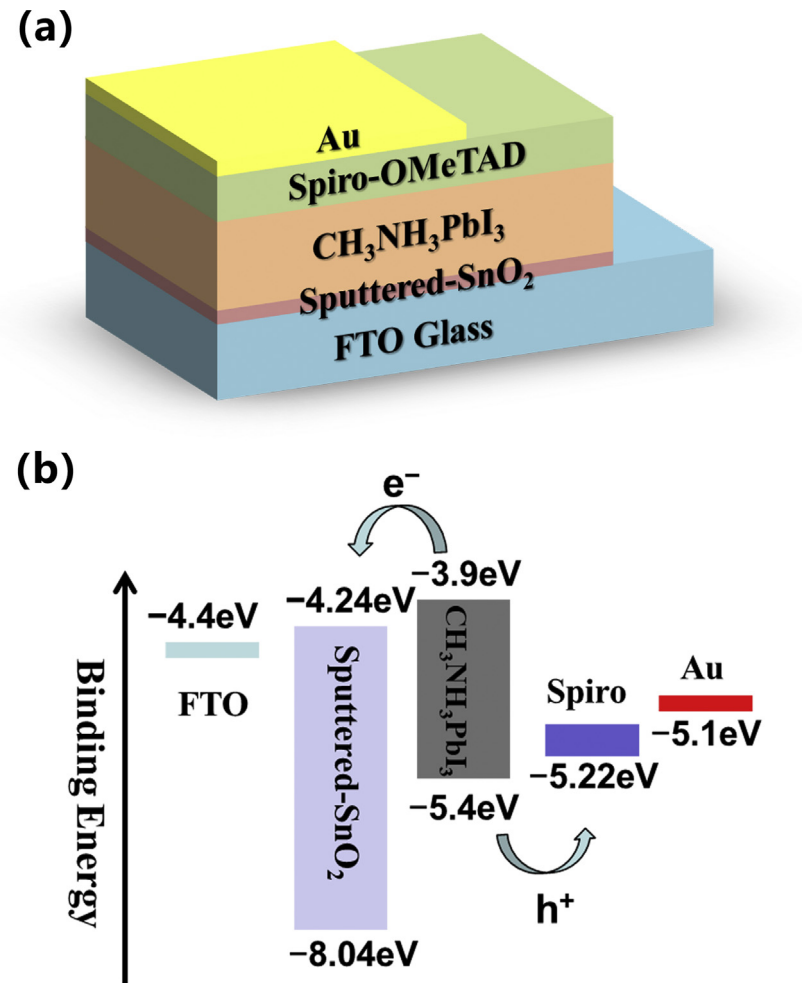

Fig. 1. (a) Structure diagram and (b) band diagram of planar PSC with sputtered SnO_2 film.

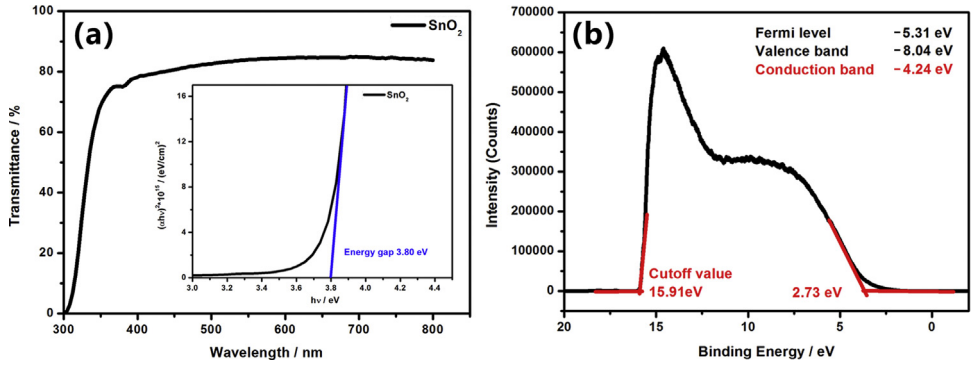

Fig. 2. (a) Transmittance spectrum and Tauc plot of SnO_2 film sputtered on glass and (b) UPS spectrum of SnO_2 film sputtered on silicon wafer.

The transmission spectrum shown in Fig. 2a demonstrates high light transmittance of sputtered SnO_2 film, which is beneficial to the light absorption of perovskite layer. And the band gap of sputtered SnO_2 film was worked out as 3.8 eV from transmission spectrum, which is shown in the inset figure [34,35]. The UPS spectrum of sputtered SnO_2 film can reflect the positions of fermi level and valence band [36]. As shown in Fig. 2b, the positions of valence band and conduction band are −8.04 eV and −4.24 eV, respectively. Fig. 1b shows the band diagram of planar PSC based on room-temperature sputtered SnO_2 film. It is obvious that the energy band structure of sputtered SnO_2 film is beneficial to the electron transport and hole blocking performances of planar PSC. The valence band of sputtered SnO_2 film is much lower than that of perovskite layer and does not allow holes in perovskite layer pass it. Therefore, room-temperature sputtered SnO_2 film can effectively act as HBL in planar PSC.

The surface image and roughness of SnO_2 film sputtered on FTO substrate were observed via AFM, and bare FTO was used as the contrast sample. As shown in Fig. 3a and b, the roughness of sample RFMS-30 is 12.9 nm, while bare FTO shows the higher roughness of 14.1 nm. It can be deduced that SnO_2 nanoparticles were deposited on the surface of FTO and refilled into gap in the grain, which is conducive to lower surface roughness of sample. In order to explore the effect of this ultrathin SnO_2 HBL on perovskite

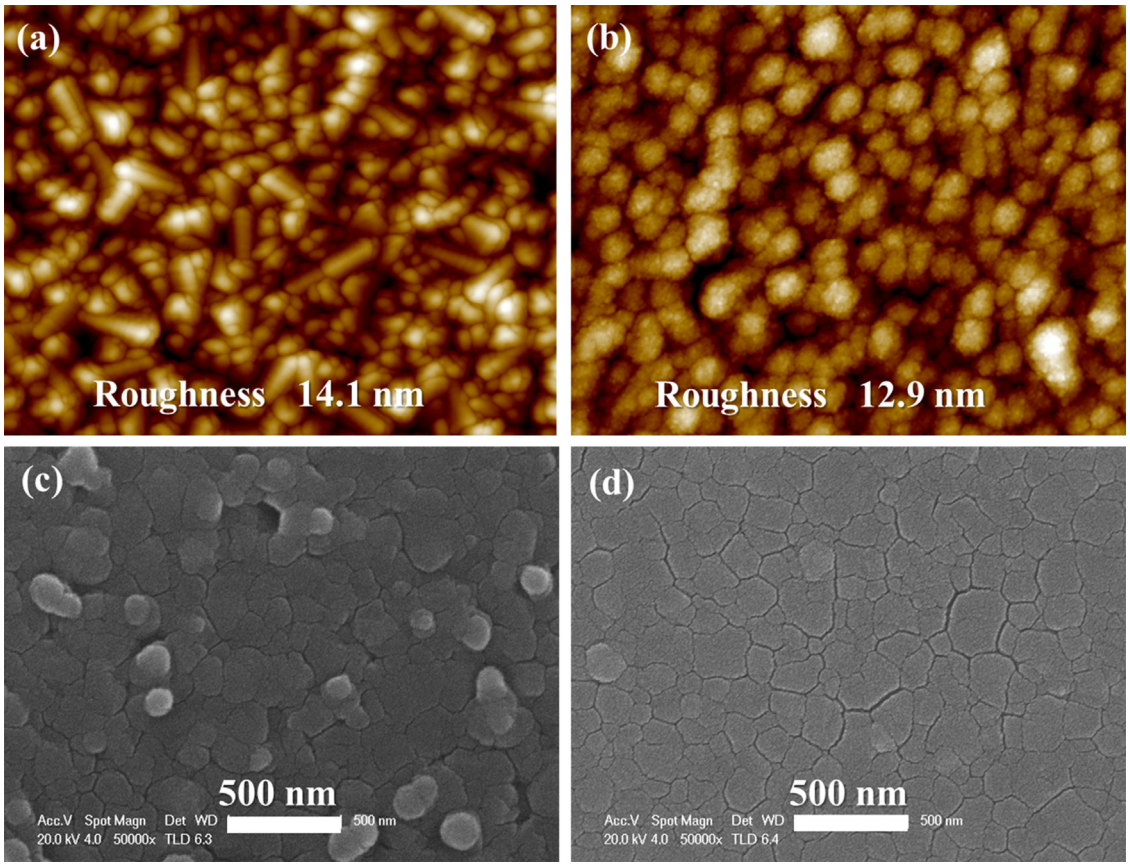

Fig. 3. AFM images of surface morphology of FTO substrate without and with sputtered SnO_2 film (a and b); SEM images of perovskite films deposited on FTO substrate without and with sputtered SnO_2 film (c and d).

layer, the surface morphologies of perovskite films deposited on different substrates were also observed. Fig. 3c and d shows SEM images of perovskite films deposited on bare FTO without and with sputtered SnO_2 film, respectively. The perovskite film deposited on bare FTO substrate is rough because of the grain precipitation and size inhomogeneity. However, perovskite layer on sputtered SnO_2 film shows smoother surface and its grain sizes are more uniform. So it can be inferred that sputtered SnO_2 underlayer has a positive effect on the following deposition of perovskite layer. It is well known that the perovskite film morphology and coverage are highly affected by the HBL/ perovskite or substrate/perovskite interface. On one hand, SnO_2 film sputtered on FTO can modify the substrate surface and provide more favorable sites for the crystallization of perovskite grains, which is beneficial to the formation of large and homogeneous perovskite grains [20–22,37]. On the other hand, as mentioned above, the reduced surface roughness caused by sputtered SnO_2 film indicates the improved surface smoothness of sample, which can contribute to the deposition of perovskite layer with large grains and low density of pinholes [38]. And the negligible number of pinholes demonstrates the high coverage of perovskite on sputtered SnO_2 film [27]. Therefore, the sputtered SnO_2 films can not only play the role of hole blocking, but also improve the crystal morphology and surface coverage of perovskite layer. Furthermore, the improvement of surface topography of perovskite layer can be beneficial to the performance of PSC, which will be furtherly verified by the photoelectric parameters of devices.

As HBL of planar PSC, the deposition rate and sputtering time of SnO_2 film are crucial to device performance. AFM measurement system was applied to analyze the deposition rate of sputtered SnO_2 film. Under the same sputtering atmosphere, potential and power, SnO_2 film was sputtered on glass substrate with sputtering time of 80 min, which is defined as sample RFMS-80. AFM measurement result shows that the thickness of sample RFMS-80 is around 50 nm. So it can be inferred that the room-temperature deposition rate of SnO_2 film is approximately 0.63 nm/min. That is to say, the thicknesses of sample RFMS-20, RFMS-30 and RFMS-40 are about 12.6, 18.9 and 25.2 nm, respectively. In addition, the effect of sputtering time on photoelectric properties of PSC was studied and the corresponding results are shown in Fig. 4a and Table 1. The efficiency of planar PSC based on bare FTO is only 5.11%, which is due to the poor short-circuit current density (J_{sc}) and fill factor (FF). After introducing sputtered SnO_2 film as HBL, the J_{sc} of devices have significant increase and exceed 19 mA/cm^2. The remarkable improvement of J_{sc} can be attributed to two factors. On one hand, sputtered SnO_2 film between FTO substrate and perovskite layer has suitable energy level of conduction band and valence band and plays an active role in promoting carrier transport and suppressing interface recombination [39]. On the other hand, as discussed above, perovskite layer on sputtered SnO_2 film is smoother than that on bare FTO, which is beneficial to improve the J_{sc} of planar PSC [28,40].

Table 1
Photoelectric parameters of different planar PSCs.

Sample	Sputtering time	*Voc*/V	*Jsc*/mA cm^{-2}	FF	PCE/%
FTO	0 min	1.01	13.01	0.39	5.11
RFMS-20	20 min	0.98	19.58	0.53	10.09
RFMS-30	30 min	1.00	20.40	0.61	12.42
RFMS-40	40 min	0.78	19.46	0.59	8.97

Through comparison, it can be concluded that 30 min is the most appropriate sputtering time and sample RFMS-30 shows the best photoelectricity performance. The FF of sample RFMS-20 is only

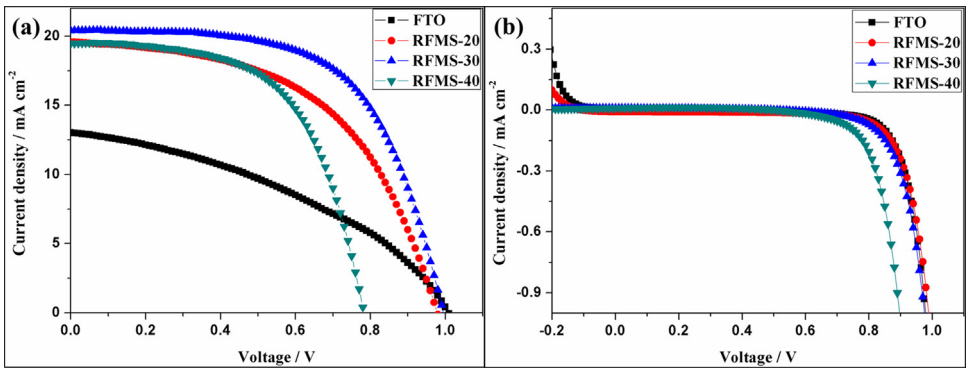

Fig. 4. J–V curves of different planar PSCs (a) under AM 1.5 illumination and (b) in dark.

Table 2
Impedance values of different planar PSCs.

Sample	R_{rec}/kΩ	R_s/Ω	R_{co}/Ω
FTO	129.00	125.10	594.42
RFMS-30	368.90	53.00	246.38

0.53, which indicates that short sputtering time affects the coverage of SnO_2 HBL and results in the direct contact between FTO substrate and perovskite layer. In addition, the low value of open circuit voltage (V_{oc}) of sample RFMS-40 leads to the sharp decline of efficiency and the decreased V_{oc} may be caused by high resistivity of sputtered SnO_2 film. The above phenomenon can be verified by the J–V curves of devices measured in dark which is shown in Fig. 4b. The leakage currents of sample FTO and RFMS-20 are very large, which illustrates low values of FF of the two samples [41]. And the small onset potential of sample RFMS-40 explains its low value of V_{oc} [42].

In addition, we utilized electrochemical impedance spectroscopy (EIS) to analyze the internal impedance changes of planar PSCs caused by sputtered SnO_2 HBL. Fig. 5a show the Nyquist plots of planar PSCs based on FTO substate with and without sputtered SnO_2 HBL measured under AM 1.5 illumination with 0 mV of bisa voltage. Nyquist plots measured under illumination condition can reflect the series resistances (R_s) and contact resistance (R_{co}) of solar cell, the high-frequency intercept on the real axis represents the value of R_s and the radius of the impedance semi-circles at high frequency represents the value of R_{co} [43,44]. The Nyquist plots of sample FTO and RFMS-30 measured in dark with 0 mV of bisa voltage are also shown in Fig. 5b. The large arc at low frequency of Nyquist plot in dark reflects the recombination resistance (R_{rec}) and the larger value of R_{rec} should lead to the less recombination [45]. Through analyzing, the corresponding impedance values of above two samples are listed in Table 2. The value of R_{rec} of planar PSC without HBL is only 129.00 kΩ, which is much smaller than that of planar PSC with sputtered SnO_2 HBL. The sample RFMS-30 has a high R_{rec} of 368.90 kΩ, which reflects the inhibiting effect of sputtered SnO_2 film on carrier recombination of planar PSC. And the significant improvement of FF caused by sputtered SnO_2 HBL can be attributed to the suppressed charge recombination [45]. In addition, the impedance semi-circle at high frequency in Nyquist plot represents R_{co} at the FTO/perovskite or SnO_2/perovskite interface. Compared with sample FTO, planar PSC with sputtered SnO_2 HBL shows a reduced value of R_{co}, which is due to the suitable energy level of conduction band of sputtering SnO_2 film [44]. The reduced R_{co} indicates the improved extraction of electrons at the SnO_2/perovskite interface and is in keeping with the increased value of J_{sc} of device. R_s represents the series resistance of device. After introducing sputtered SnO_2 HBL, the value of R_s of planar PSC decreases from 125.10 Ω to 53.00 Ω. This phenomenon confirms that sputtered SnO_2 HBL has a positive effect on decreasing interface recombination, improving electron extraction and hole-blocking performance of planar PSC. That is to say, the increased R_{rec}, decreased R_s and R_{co} explain well the optimized values of J_{sc} and FF of devices and confirm the effect of SnO_2 HBL sputtered at room temperature.

In order to further analyze the effect of sputtered SnO_2 HBL on planar PSC, we measured the open circuit voltage decay (OCVD) curves of planar PSCs based on FTO substrate with and without sputtered SnO_2 HBL. As shown in Fig. 6a, after turning off illumination, the V_{oc} of sample RFMS-30 declines more slowly than that of sample FTO. The electron lifetime of above samples can be calculated from OCVD curves and the relevant results are shown in Fig. 6b. It is obvious that the electron lifetime of sample RFMS-30 is much longer than that of sample FTO, which further confirms the effect of room-temperature sputtered SnO_2 film as HBL in planar PSC.

The improvements of photoelectric properties caused by sputtered SnO_2 HBL are mainly due to the enhancements of J_{sc} and FF. Therefore, we measured the external quantum efficiency (EQE) curves of planar PSCs with and without sputtered SnO_2 HBL that is shown in Fig. 7a. It is obvious that sputtered SnO_2 HBL greatly improves the intensity and range of EQE curve of PSC. On one hand, the improved deposition of perovskite layer caused by sputtered SnO_2 HBL could enhance the light absorption property of device. On the other hand, room-temperature sputtered SnO_2 HBL, as an interface layer between FTO substrate and perovskite film, greatly improves the carrier transport and hole blocking performance of PSC. The estimated value of J_{sc} of sample RFMS-30 is figured out to be 20.78 mA/cm^2 by the fitting analysis of EQE curve and it is close to the experiment value. This further verifies that SnO_2 film prepared by RFMS method at room temperature is a promising HBL material for PSC. What's more, through optimizing the deposition of perovskite layer, we obtained the best photoelectric efficiency of sample RFMS-30 which is shown in Fig. 7b. The values of V_{oc}, J_{sc}, FF and efficiency (PCE) are 1.03 V, 20.06 mA/cm^2, 0.66 and 13.68%, respectively.

In addition, in order to verify the repeatability of planar PSC based on room-temperature sputtered SnO_2 HBL, J–V curves of 30 devices with SnO_2 HBL sputtered at room temperature were measured. Fig. 8 shows the histograms of V_{oc}, J_{sc}, FF and PCE of 30 planar PSCs. These histograms can reflect the average performance of devices. The average values of V_{oc}, J_{sc}, FF and PCE are around 1 V, 20.3 mA/cm^2, 0.6 and 12%, respectively. This result demonstrates that planar PSC based on room-temperature sputtered SnO_2 HBL has a good repeatability.

The comparisons of SnO_2 films obtained by different methods and related device performances are listed in Table S1 [21,24–26,46–47]. As shown in Table S1, the preparation meth-

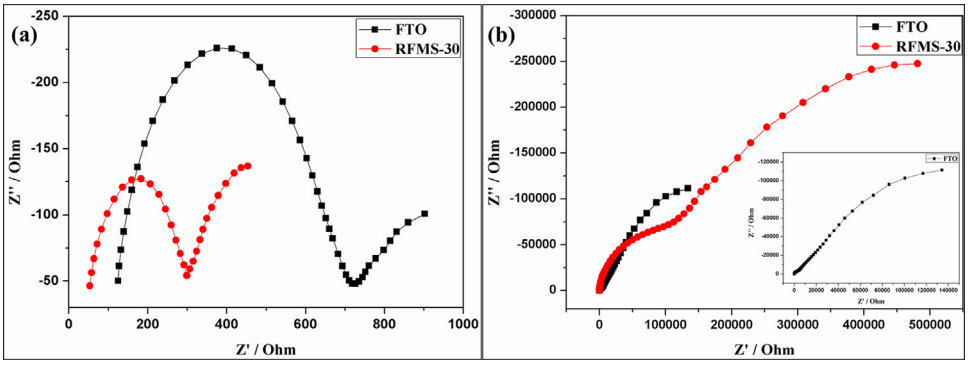

Fig. 5. Nyquist plots of different planar PSCs measured (a) under AM 1.5 illumination with 0 mV of bisa voltage and (b) in dark with 0 mV of bisa voltage.

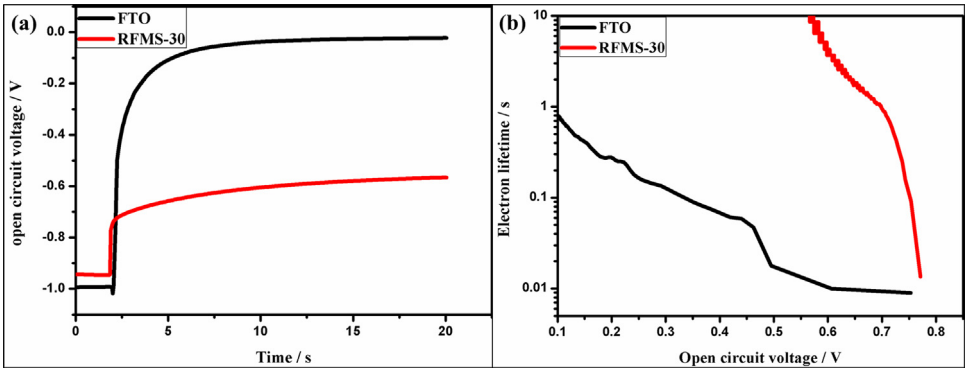

Fig. 6. (a) OCVD curves and (b) electron lifetime curves as a function of open circuit voltage for different planar PSCs.

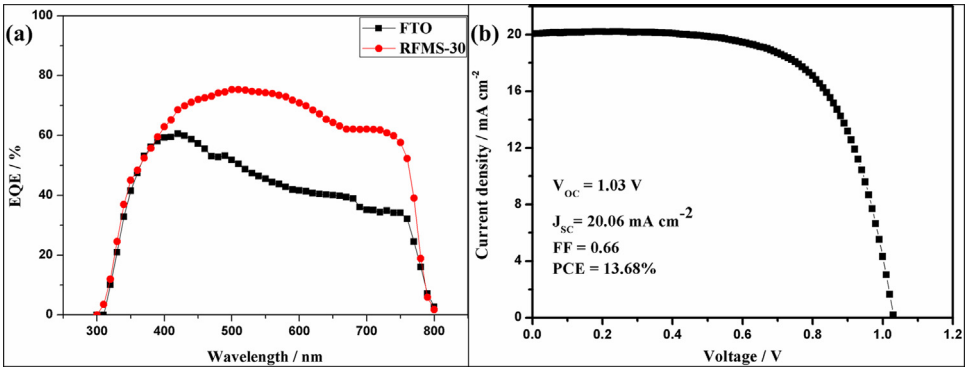

Fig. 7. (a) External quantum efficiency (EQE) curves of different planar PSCs and (b) J–V curve of the best planar PSC based on room-temperature sputtered SnO_2 film.

ods of SnO_2 HBL are various and all below 200 °C. As reported by Fang [46], PSCs based on high crystalline SnO_2 films sintered at high-temperature even exhibited the worse photoelectric properties. And these related reports support the feasibility of room-temperature processed SnO_2 HBL. Compared with other methods, room-temperature sputtering method without sintering in this work shows some advantages such as easy-operation, low-cost and celerity. In terms of film thickness, it is obvious that the thicknesses of SnO_2 layers are mostly controlled very thin in order to optimize the efficiencies of PSCs. Taking into consideration the compositions of perovskite layers and performances of PSCs, it is found that mixed halide/cation perovskite material makes PSC based on SnO_2 HBL achieve the best photoelectric performance in Table S1 [24], which indicates the importance of interaction between SnO_2 film and perovskite material. In conclusion, the PSC based on room-temperature sputtered SnO_2 HBL exhibits favorable performance, and relevance research of sputtered SnO_2 HBL and perovskite material is required in the future.

4. Conclusion

In conclusion, this research illustrates the potential application of SnO_2 film sputtered at room temperature as HBL in planar PSC. SnO_2 film prepared by RFMS method shows high mobility, high transmittance and suitable energy band structure for planar PSC. The ultrathin sputtered SnO_2 film between FTO substrate and perovskite layer can effectively improve the performance of electron extraction and hole blocking of planar PSC because of the preferable energy band structure. In addition, room-temperature sputtered SnO_2 HBL can also improve the smoothness of perovskite layer, which is helpful to increase value of J_{sc}. These optimizations of photoelectric properties are well explained by the increased R_{rec}, decreased R_s and R_{co} of devices. And the remarkable enhance-

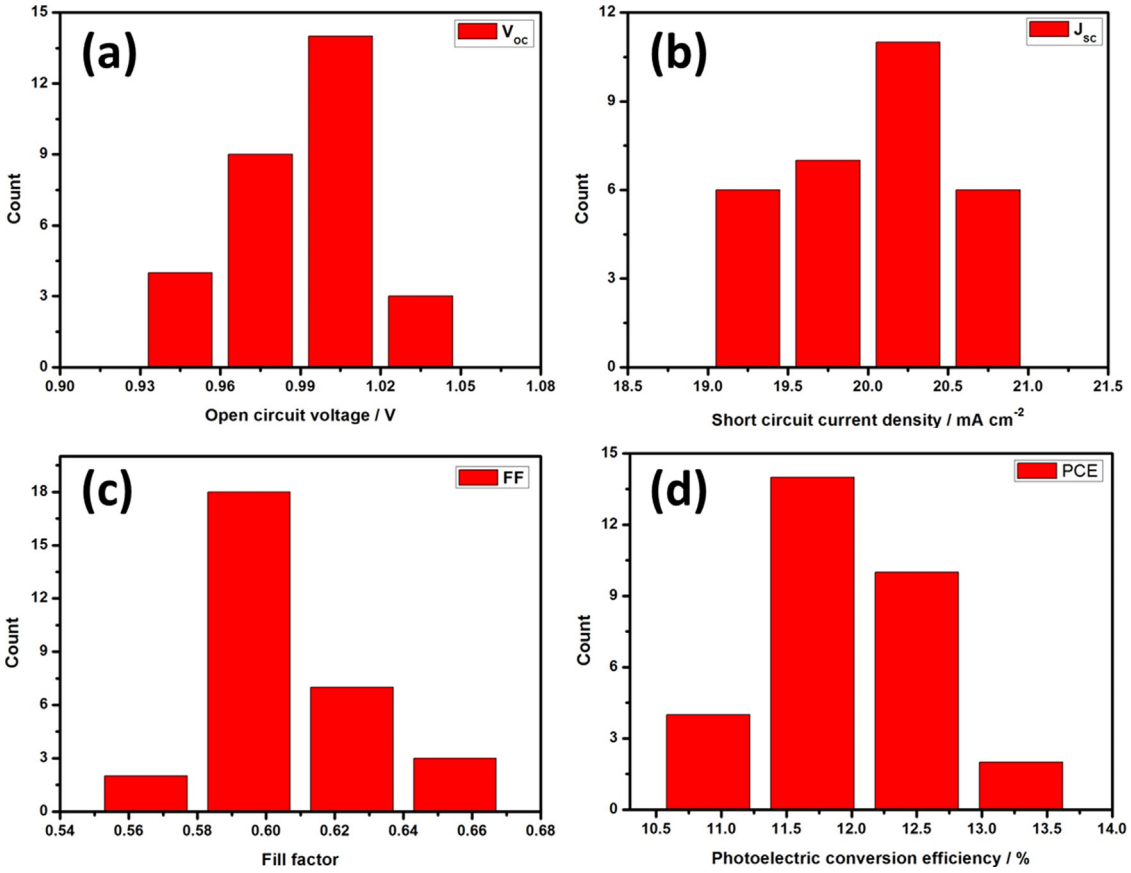

Fig. 8. Histograms of (a) V_{oc}, (b) J_{sc}, (c) FF and (d) PCE of 30 PSCs based on SnO_2 HBL sputtered at room temperature.

ment of J_{SC} caused by sputtered SnO_2 HBL is corresponding to EQE results. What's more, the planar PSCs with sputtered SnO_2 HBL also show good repeatability. After optimization, the planar PSC with room-temperature sputtered SnO_2 HBL obtains the best efficiency of 13.68%. Notably, both the room temperature preparation process and excellent properties of SnO_2 HBL can help to realize the fabricated technology of PSC at low temperature and improve the applicability of PSC.

Acknowledgments

This work was financially supported by the National High Technology Research and Development Program (2015AA050601), the Scientific Research Fund Project of Wuhan Institute of Technology (K201703), the Fundamental Research Funds for the Central Universities, South-Central University for Nationalities (CZQ16003), the State Key Laboratory of Crystal Materials, Shandong University (KF1612) and the National Natural Science Foundation of China (Nos. 11704418, 11575134, 11504436).

Appendix A. Supplementary data

Supplementary material related to this article can be found, in the online version, at doi:https://doi.org/10.1016/j.apsusc.2017.11.161

References

[1] H.S. Kim, C.R. Lee, J.H. Im, K.B. Lee, T. Moehl, A. Marchioro, S.J. Moon, R. Humphry-Baker, J.H. Yum, J.E. Moser, Lead iodide perovskite sensitized all-solid-state submicron thin film mesoscopic solar cell with efficiency exceeding 9%, Sci. Rep. 2 (2012) 591.
[2] M.M. Lee, J. Teuscher, T. Miyasaka, T.N. Murakami, H.J. Snaith, Efficient hybrid solar cells based on meso-superstructured organometal halide perovskites, Science 338 (2012) 643.
[3] M. Liu, M.B. Johnston, H.J. Snaith, Efficient planar heterojunction perovskite solar cells by vapour deposition, Nature 501 (2013) 395.
[4] H. Zhou, Q. Chen, G. Li, S. Luo, T.B. Song, H.S. Duan, Z. Hong, J. You, Y. Liu, Y. Yang, Interface engineering of highly efficient perovskite solar cells, Science 345 (2014) 542–546.
[5] N. Ahn, D.Y. Son, I.H. Jang, S.M. Kang, M. Choi, N.G. Park, Highly reproducible perovskite solar cells with average efficiency of 18.3% and best efficiency of 19.7% fabricated via Lewis base adduct of lead(II) iodide, J. Am. Chem. Soc. 137 (2015) 8696–8699.
[6] W.S. Yang, B.W. Park, E.H. Jung, N.J. Jeon, Y.C. Kim, D.U. Lee, S.S. Shin, J. Seo, E.K. Kim, J.H. Noh, S. Seok, Iodide management in formamidinium lead halide based perovskite layers for efficient solar cells, Science 356 (2017) 1376–1379.
[7] S.D. Stranks, G.E. Eperon, G. Grancini, C. Menelaou, M.J. Alcocer, T. Leijtens, L.M. Herz, A. Petrozza, H.J. Snaith, Electron-hole diffusion lengths exceeding 1 micrometer in an organometal trihalide perovskite absorber, Science 342 (2013) 341–344.
[8] D. Guo, J. Yu, K. Fan, H. Zou, B. He, Nanosheet-based printable perovskite solar cells, Sol. Energy Mater. Sol. Cells 159 (2017) 518–525.
[9] P. Tiwana, P. Docampo, M.B. Johnston, H.J. Snaith, L.M. Herz, Electron mobility and injection dynamics in mesoporous ZnO, SnO_2, and TiO_2 films used in dye-sensitized solar cells, ACS Nano 5 (2011) 5158–5166.
[10] J.W. Lee, T.Y. Lee, P.J. Yoo, M. Grätzel, S. Mhaisalkar, N.G. Park, Rutile TiO_2-based perovskite solar cells, J. Mater. Chem. A 2 (2014) 9251–9259.
[11] K. Wojciechowski, M. Saliba, T. Leijtens, A. Abate, H.J. Snaith, Sub-150 °C processed meso-superstructured perovskite solar cells with enhanced efficiency, Energy Environ. Sci. 7 (2014) 1142–1147.
[12] C. Chen, Y. Cheng, Q. Dai, H. Song, Radio frequency magnetron sputtering deposition of TiO_2 thin films and their perovskite solar cell applications, Sci. Rep. 5 (2015) 17684.
[13] C. Liang, Z. Wu, P. Li, J. Fan, Y. Zhang, G. Shao, Chemical bath deposited rutile TiO_2 compact layer toward efficient planar heterojunction perovskite solar cells, Appl. Surf. Sci. 391 (2017) 337–344.
[14] B. Roose, K. Gödel, S. Pathak, A. Sadhanala, J. Baena, B. Wilts, H.J. Snaith, U. Wiesner, M. Grätzel, U. Steiner, A. Abate, Enhanced efficiency and stability of perovskite solar cells through Nd-doping of mesostructured TiO_2, Adv. Energy Mater. 6 (2016) 1501868.

[15] D.H. Lee, D. Song, Y.S. Kang, W.I. Park, Three-dimensional monolayer graphene and TiO_2 hybrid architectures for high-efficiency electrochemical photovoltaic cells, J. Mater. Chem. C 119 (2015) 6880–6885.
[16] S. Bao, J. Wu, X. He, Y. Tu, S. Wang, M. Huang, Z. Lan, Mesoporous Zn_2SnO_4 as effective electron transport materials for high-performance perovskite solar cells, Electrochim. Acta 251 (2017) 307–315.
[17] K. Wang, Y. Shi, Q. Dong, Y. Li, S. Wang, X. Yu, M. Wu, T. Ma, Low-temperature and solution-processed amorphous WO_X as electron-selective layer for perovskite solar cells, J. Phys. Chem. Lett. 6 (2015) 755–759.
[18] M. Qin, J. Ma, W. Ke, P. Qin, H. Lei, H. Tao, X. Zheng, L. Xiong, Q. Liu, Z. Chen, J. Lu, G. Yang, G. Fang, Perovskite solar cells based on low-temperature processed indium oxide electron selective layers, ACS Appl. Mater. Interfaces 8 (2016) 8460–8466.
[19] Y. Xu, T. Liu, Z. Li, B. Feng, S. Li, J. Duan, C. Ye, J. Zhang, H. Wang, Preparation and photovoltaic properties of perovskite solar cell basedon ZnO nanorod arrays, Appl. Surf. Sci. 388 (2016) 89–96.
[20] W. Ke, G. Fang, Q. Liu, L. Xiong, P. Qin, H. Tao, J. Wang, H. Lei, B. Li, J. Wan, Low-temperature solution-processed tin oxide as an alternative electron transporting layer for efficient perovskite solar cells, J. Am. Chem. Soc. 137 (2015) 6730–6733.
[21] J. Song, E. Zheng, J. Bian, X.F. Wang, W. Tian, Y. Sanehira, T. Miyasaka, Low-temperature SnO_2-based electron selective contact for efficient and stable perovskite solar cells, J. Mater. Chem. A 3 (2015) 10837–10844.
[22] Q. Jiang, L. Zhang, H. Wang, X. Yang, J. Meng, H. Liu, Z. Yin, J. Wu, X. Zhang, J. You, Enhanced electron extraction using SnO_2 for high-efficiency planar-structure $HC(NH_2)_2PbI_3$-based perovskite solar cells, Nat. Energy 1 (2016) 16177.
[23] J. Duan, Q. Xiong, B. Feng, Y. Xu, J. Zhang, H. Wang, Low-temperature processed SnO_2 compact layer for efficient mesostructure perovskite solar cells, Appl. Surf. Sci. 391 (2017) 677–683.
[24] J.P.C. Baena, L. Steier, W. Tress, M. Saliba, S. Neutzner, T. Matsui, F. Giordano, T.J. Jacobsson, A.R.S. Kandada, S.M. Zakeeruddin, Highly efficient planar perovskite solar cells through band alignment engineering, Energy Environ. Sci. 8 (2015) 2928–2934.
[25] M. Abulikemu, M. Neophytou, J.M. Barbé, M.L. Tietze, A. El Labban, D.H. Anjum, A. Amassian, I. McCulloch, S. Del Gobbo, Microwave-synthesized tin oxide nanocrystals for low-temperature solution-processed planar junction organo-halide perovskite solar cells, J. Mater. Chem. A 5 (2017) 7759–7763.
[26] J.Y. Chen, C.C. Chueh, Z. Zhu, W.C. Chen, A.K.Y. Jen, Low-temperature electrodeposited crystalline SnO_2 as an efficient electron-transporting layer for conventional perovskite solar cells, Sol. Energy Mater. Sol. Cells 164 (2017) 47–55.
[27] S. Ge, H. Xu, W. Wang, R. Cao, Y. Wu, W. Xu, J. Zhu, F. Xue, F. Hong, R. Xu, The improvement of open circuit voltage by the sputtered TiO_2 layer for efficient perovskite solar cell, Vacuum 128 (2016) 91–98.
[28] H. Tao, W. Ke, J. Wang, Q. Liu, J. Wan, G. Yang, G. Fang, Perovskite solar cell based on network nanoporous layer consisted of TiO_2 nanowires and its interface optimization, J. Power Sources 290 (2015) 144–152.
[29] W.C. Lai, K.W. Lin, T.F. Guo, P. Chen, Y.T. Wang, Conversion efficiency improvement of inverted $CH_3NH_3PbI_3$ perovskite solar cells with room temperature sputtered ZnO by adding the C60 interlayer, Appl. Phys. Lett. 107 (2015), 114-111.
[30] S.S. Malia, C.K. Hong, A.I. Inamdar, H. Im, S.E. Shim, Efficient planar n-i-p type heterojunction flexible perovskite solar cells with sputtered TiO_2 electron transporting layers, Nanoscale 9 (2017) 3095–3104.
[31] W. Yang, Y. Yao, C.Q. Wu, Mechanism of charge recombination in meso-structured organic-inorganic hybrid perovskite solar cells: a macroscopic perspective, J. Appl. Phys. 117 (2015) 155504.
[32] G.S. Han, Y.H. Song, Y.U. Jin, J.W. Lee, N.G. Park, B.K. Kang, J.K. Lee, I.S. Cho, D.H. Yoon, H.S. Jung, Reduced graphene oxide/mesoporous TiO_2 nanocomposite based perovskite solar cells, ACS Appl. Mater. Interfaces 7 (2015) 23521–23526.
[33] H.W. Lei, G. Yang, Y.X. Guo, L.B. Xiong, P.L. Qin, X. Dai, X.L. Zheng, W.J. Ke, H. Tao, Z. Chen, B.R. Li, G.J. Fang, Efficient planar Sb_2S_3 solar cells using a low-temperature solution-processed tin oxide electron conductor, Phys. Chem. Chem. Phys. 18 (2016) 16436–16443.
[34] J. Wei, J.M. Murray, J. Barnes, L.P. Gonzalez, S. Guha, Determination of the temperature dependence of the band gap energy of semiconductors from transmission spectra, J. Electron. Mater. 41 (2012) 2857–2866.
[35] Y. Wang, W. Tang, L. Zhang, J. Zhao, Electron concentration dependence of optical band gap shift in Ga-doped ZnO thin films by magnetron sputtering, Thin Solid Films 565 (2014) 62–68.
[36] C.F. Chi, H.W. Cho, H. Teng, C.Y. Chuang, Y.M. Chang, Y.J. Hsu, Y.L. Lee, Energy level alignment, electron injection, and charge recombination characteristics in CdS/CdSe cosensitized TiO_2 photoelectrode, Appl. Phys. Lett. 98 (2011) 012101.
[37] Y. Hou, J.Y. Yang, Q.H. Jiang, W.X. Li, Z.W. Zhou, X. Li, S.Q. Zhou, Enhancement of photovoltaic performance of perovskite solar cells by modification of the interface between the perovskite and mesoporous TiO_2 film, Sol. Energy Mater. Sol. Cells 155 (2016) 101–107.
[38] W.J. Ke, G.J. Fang, J.W. Wan, H. Tao, Q. Liu, L.B. Xiong, P.L. Qin, J. Wang, H.W. Lei, G. Yang, M.C. Qin, X.Z. Zhao, Y.F. Yan, Efficient hole-blocking layer-free planar halide perovskite thin-film solar cells, Nat. Commun. 6 (2015) 6700.
[39] H.S. Rao, B.X. Chen, W.G. Li, Y.F. Xu, H.Y. Chen, D.B. Kuang, C.Y. Su, Improving the extraction of photogenerated electrons with SnO_2 nanocolloids for efficient planar perovskite solar cells, Adv. Funct. Mater. 25 (2015) 7200–7207.
[40] C.Y. Chang, C.Y. Chu, Y.C. Huang, C.W. Huang, S.Y. Chang, C.A. Chen, C.Y. Chao, W.F. Su, Tuning perovskite morphology by polymer additive for high efficiency solar cell, ACS Appl. Mater. Interfaces 7 (2015) 4955–4961.
[41] B.J. Richardson, L. Zhu, Q. Yu, Inverted hybrid solar cells based on pyrite FeS_2 nanocrystals in P_3HT:PCBM with enhanced photocurrent and air-stability, Sol. Energy Mater. Sol. Cells 116 (2013) 252–261.
[42] C. Zhou, J. Ouyang, B. Yang, Retarded hydrolysis-condensing reactivity of tetrabutyl titanate by acetylacetone and the application in dye-sensitized solar cells, Mater. Res. Bull. 48 (2013) 4351–4356.
[43] Y. Tu, J. Wu, M. Zheng, J. Huo, P. Zhou, Z. Lan, J. Lin, M. Huang, TiO_2 quantum dots as superb compact block layers for high-performance $CH_3NH_3PbI_3$ perovskite solar cells with an efficiency of 16.97%, Nanoscale 7 (2015) 20539–20546.
[44] D. Liu, J. Yang, T.L. Kelly, Compact layer free perovskite solar cells with 13.5% efficiency, J. Am. Chem. Soc. 136 (2014) 17116–17122.
[45] P. Chen, Z. Jin, Y. Wang, M. Wang, S. Chen, Y. Zhang, L. Wang, X. Zhang, Y. Liu, Interspace modification of titania-nanorod arrays for efficient mesoscopic perovskite solar cells, Appl. Surf. Sci. 402 (2017) 86–91.
[46] W. Ke, D. Zhao, A. Cimaroli, C. Grice, P. Qin, Q. Liu, L. Xiong, Y. Yan, G. Fang, Effects of annealing temperature of tin oxide electron selective layers on the performance of perovskite solar cells, J. Mater. Chem. A 3 (2015) 24163–24168.
[47] X. Liu, K. Tsai, Z.L. Zhu, Y. Sun, C. Chueh, A.K. Jen, A low-temperature, solution processable tin oxide electron-transporting layer prepared by the dual-fuel combustion method for efficient perovskite solar cells, Adv. Mater. Interfaces 3 (2016) 1600122.